Journal of The Electrochemical Society, **154** (10) B1041-B1048 (2007)
0013-4651/2007/154(10)/B1041/8/$20.00 © The Electrochemical Society

Analysis of the Key Parameters in the Cold Start of Polymer Electrolyte Fuel Cells

Yun Wang[*,z]

Renewable Energy Resources Lab and National Fuel Cell Research Center, Department of Mechanical and Aerospace Engineering, The University of California, Irvine, Irvine, California 92612, USA

This paper investigates the heat/mass transfer and electrochemical kinetics in the cathode catalyst layer of polymer electrolyte fuel cells (PEFCs) during cold start below the freezing temperature. A number of key parameters that govern the cold-start operations, such as time constants and the Damköhler number, are defined and their impacts are explored. A lumped parameter model for cell temperature and ice formation is developed and one-dimensional analysis is performed on the reactant transport in the catalyst layer. We found that a dimensionless parameter, defined as ratio of the time constant of cell warmup to that of ice-volume growth, is important for self-startup of fuel cells in subzero conditions, and a high value of tortuosity has profound impact on reactant starvation during cold start. In addition, the reduction in the electrochemical active surface of the catalyst layer due to the ice coverage is found to be a major mechanism leading to cell voltage loss during cold start.
 [DOI: 10.1149/1.2767849]

Manuscript submitted April 6, 2007; revised manuscript received June 4, 2007. Available electronically August 16, 2007.

Cold-start (subzero startup) capability of polymer electrolyte fuel cells (PEFCs) is of paramount importance for PEFC automobile applications. During startup in subzero environments, produced water in the electrodes may freeze instantaneously at the reaction sites, covering and hence reducing the electrochemical active surface as well as plugging the open pores of reactant passage. To ensure a successful startup below the freezing point, the fuel cell needs to be heated, by either external heat source or self-heating, to at least 0°C before the solid water in the catalyst layer causes severe reactant starvation and considerable reactive area reduction and a consequent substantial voltage loss. In automobile applications, such a startup must be short (less than minutes) in order to compete with the traditional internal combustion engines.

Though much research has been carried out to characterize the steady-state operation and the transient operation (>0°C),[1] the physics during cold-start operation is poorly understood despite its importance in fuel cell deployment. One of the first studies on cold start was conducted by Hishinuma et al.,[2] McDonald et al.,[3] and Cho et al.[4] Hishinuma et al.[2] studied the performance of a single cell under a variety of operating conditions during cold start (from -25 to -3°C). They found that the performance of a PEFC decreases due to ice formation on the reactive area of the cathode and heat generated by fuel cells might be enough to warm up the cell from cold start at -5°C and make self-starting possible. They also indicated that it is necessary to heat the cell with external sources in order to make a startup below -5°C. McDonald et al.[3] conducted an experimental study to investigate the physical changes in fuel cell membranes arising from freeze/thaw cycling. They considered hundreds of temperature cycles between 80 and -40°C over months. Cho et al.[4] carried out a study on cell degradation related to the thermal cycle. They ran fuel cells at 80°C, stopped, cooled to a subzero condition, and reheated to 80°C for another thermal cycle. They found that the observed degradation was attributed to freezing of water that was produced during operation and remained in the PEFC after the operation. By using the gas-purging method, they successfully reduced the degradation rate.

Recently, Oszcipok et al.[5] conducted isothermal potentiostatic cold start measurements of fuel cells under various operating conditions and found that water freezes in the porous structures of the cathode electrode, the microporous layer, and the gas diffusion layer (GDL). They also carried out statistic evaluation of the experiments, which indicated that dryer membranes and high air-flow rates are beneficial for high charge-transfer rates. Yana et al.[6] investigated the effect of subfreezing temperatures on cell performance and components. They showed that fuel cells were able to start at -5°C after being prepurged and insulated, and with the higher air stoichiometry and higher feed gas temperature at -10°C, it was possible to make a startup at low current densities (<0.1 A/cm^2). They also found delamination of the catalyst layer from both the membrane and GDL during cold-start operations.

The modeling work of cold start was attempted by He and Mench[7] and Mao and Wang.[8] He et al.[7] presented a 1D transient model to describe the water migration and ice-lens formation process. They found that the Nafion thickness and initial water content might have a direct effect on the potential damage to delamination between the Nafion and catalyst layer. The multidimension model of Mao and Wang[8] was built upon the transient model of Wang and Wang,[9,10] by incorporating the mechanisms of ice formation. They explored the effects of startup current density and membrane thickness on cell performance during cold start.

In addition to the cell performance during cold start, Saito et al.[11] and Cappadonia et al.[12] conducted a study with focus on the membrane at low temperatures. Saito et al.[11] investigated the temperature dependence of the ion and water transport in several types of membranes. They found that a portion of water is frozen around -20°C, but nonfreezing water remains and is able to transport in the membrane. Cappadonia et al.[12] employed impedance spectroscopy to study the conductance of Nafion membranes as a function of temperature. They measured the conductance of Nafion membranes in a wide range of temperatures down to the subzero regime.

Despite the efforts in previous studies, the following aspects of fundamental research are still highly needed for cold start. One is to elucidate the electrochemical and transport mechanisms during cold start; the other is to investigate the key physical parameters that characterize the PEFC cold start and the mechanisms that govern the voltage loss. In this paper, characterization of heat and water transport in fuel cells is presented for development of a lumped parameter thermal/water model. Analysis of the key parameters such as time scales is conducted and physics of oxygen transport and overpotential behaviors in the catalyst layer are investigated.

Modeling and Theoretical Analysis

Characterization of Heat Transfer.— Figure 1 schematically shows the components of a PEFC in one dimension. To investigate the spatial variation of temperature in a fuel cell at cold start, we follow the heat-analysis approach outlined in Ref. 13 and 14 and characterize the heat sources during cold start to two categories: the heat produced only in the catalyst layer and that in most parts of fuel cells. The primary thermal source in the second category is the ohmic heat $[(i_e^2/\kappa^{eff}) + (i_s^2/\sigma^{eff})]$ and is fairly small at low current densities. Considering a typical resistance of 100 mΩ cm^2, the ratio of ohmic heat release to the power density $I \times V_{cell}$ is less than 2%

* Electrochemical Society Active Member.
z E-mail: yunw@uci.edu

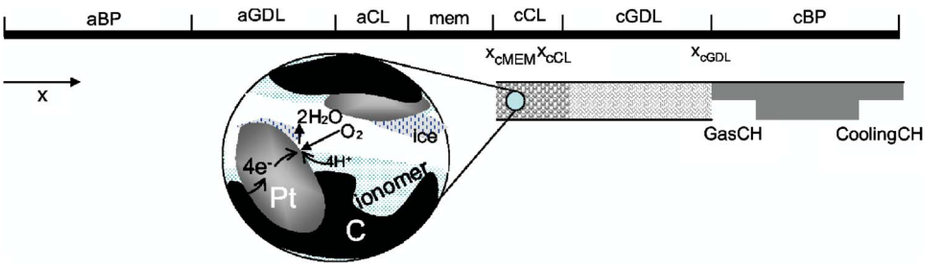

Figure 1. (Color online) Schematic of PEFC in one dimension.

at current density of 0.1 A/cm^2. Two major sources in the first category are the reaction heat $j[\eta + T(dU_o/dT)]$ and latent heat of phase change $h_{sg}\dot{m}_{sg}$. These heating mechanisms primarily take place at the reaction surface within the catalyst layer. Neglecting the ohmic heat, the variation of temperate across the catalyst layer can be estimated by employing the total heat release, S_T

$$\Delta T_{CL} \sim \frac{\delta_{CL}^2 S_T}{k_{CL}^{eff}} = \frac{\delta_{CL} I(E_o - Vcell)}{k_{CL}^{eff}} \quad [1]$$

where E_o is defined as $-(\Delta\bar{h}/2F)$ and represents the electromotive force (EMF) that all the energy from hydrogen/oxygen, the "calorific value," heating value, or enthalpy of formation, were transformed into electrical energy with the ice as the reaction product.[15] The value of E_o also considers the latent heats of fusion and condensation as well as the sensible heat. $E_o = 1.25$ and 1.48 V for low-heat value (LHV) and high-heat value (HHV),[15] respectively, while $E_o \approx 1.53$ V during cold start. Typically, the effective conductivity, k^{eff}, is around 3.0 W/m K, leading to $\Delta T_{CL} \approx 0.003$ K at 0.1 A/cm^2. Similarly, ΔT_{GDL} and ΔT_{BP} are both <0.05 K. Therefore, temperature can be assumed uniform in a fuel cell during cold start. The cell temperature can then be obtained through conservation of thermal energy

$$T = \frac{\int_0^t [I(E_o - Vcell)A_m + \Delta\dot{Q}_{gasflow} + \Delta\dot{Q}_{coolant} - \dot{Q}_{loss}]dt}{m_m Cp_m + m_{CL}Cp_{CL} + m_{GDL}Cp_{GDL} + m_{BP}Cp_{BP}} + T_o \quad [2]$$

where T_o is the initial temperature. Considering the case of self-heating and no heat loss, the time constant of cell warmup to the freezing temperature can be estimated by

$$\int_0^{\tau_{T,1}} (E_o - Vcell)dt = \frac{(m_m Cp_m + m_{CL}Cp_{CL} + m_{GDL}Cp_{GDL} + m_{BP}Cp_{BP})(273.15 - T_o)}{A_m I} \quad [3]$$

Typically, the value of $m_{BP}Cp_{BP}$ is much larger than the summation of the others. Neglecting other parts and assuming a constant heat generation, one obtains

$$\tau_{T,1} = \frac{\rho_{BP}Cp_{BP}\delta_{BP}}{I(E_o - Vcell)}(273.15 - T_o) \quad [4]$$

where the effective length of bipolar plates, δ_{BP}, is defined as $m_{BP}/A_m\rho_{BP}$. Typically, $\rho_{BP}Cp_{BP}$ is $\sim$1600 kJ/K m^3, δ_{BP} is $\sim$0.02 m, and I is 0.1 A/cm^2, yielding $\tau_{T,1} \sim 100$ s for cold start at -30°C. Considering $m_{GDL}Cp_{GDL}/m_{BP}Cp_{BP} \sim 0.03$, it takes about a few seconds ($\sim$3 s) to solely heat the GDLs to the freezing point. The geometrical physical and operating parameters are shown in Table I.

Characterization of water transport.— Water gained in the cathode catalyst layer can be expressed as

$$\iiint_{CL} S^w dv = \iiint_{CL} S_{prod} dv + \iiint_{CL} S_{EOD} dv - \iint_{MEM-CL} \vec{G}_{MEM} \cdot d\vec{s} - \iint_{GDL-CL} \vec{G}_{GDL} \cdot d\vec{s} \quad [5]$$

where $S_{prod} = -(j_c/2F)$, $S_{EOD} = -\nabla \cdot [(n_d/F)i^\omega] = -\bar{n}_d(j_c/F)$, and j_c is transfer current density at the reaction site. Note that the electro-osmatic drag (EOD), n_d, may be a function of water content. For analysis purposes, we use a constant value of $\bar{n}_d$. $\vec{G}_{MEM}$ represents the amount of water flux back to the membrane, either hydrating the electrolyte or compensating for water loss in the anode. At steady state, a coefficient α is used to indicate water transfer between the anode and cathode. Here, we still use this term to show the net water gain in the cathode in addition to the water production during cold start. Note that the coefficient α here combines the effects of the water exchange between the two sides as well as the water absorbed/released by the ionomer membrane. In addition, α can vary with time. For analysis purposes, we use a constant value (or the time average) of α. Assuming no spatial variations, i.e., $\iint_{CL}[]dv = [] \times V_{CL}$, the first three terms at the right side of Eq. 5 can be expressed as

$$-(1 + 2\alpha)\frac{j_c}{2F}V_{CL} = (1 + 2\alpha)\frac{I}{2F}A_m \quad [6]$$

The water flux across the interface between the catalyst layer and GDL is calculated by $\vec{G}_{GDL} = [-D^{w,eff} \nabla C^w + \vec{u}C^w]_{GDL-CL}$. For the traditional design of PEFC flow fields, diffusion dominates reactant transport in the GDL,[16] while for the interdigitated flow field[17] or the one in Ref. 18, convection can be the dominant mechanism in the GDLs. Assuming no ice or liquid water formation in the GDL, conservation of water in the cathode channel and GDL yields

$$\iint_{GDL-CL} \vec{G}_{GDL} d\vec{s} = \iint_{outlet} \vec{u}C^w d\vec{s} + \iint_{inlet} \vec{u}C^w d\vec{s} = \frac{IA_m}{F}\frac{\xi_c(\bar{C}^w_{c,out} - \bar{C}^w_{c,in})}{4C^{O_2}_{c,in}} \quad [7]$$

where $\bar{C}$ is the average value, defined by $\iint \vec{u}Cd\vec{s}/|\iint_{inlet}\vec{u}d\vec{s}|$. If this flux term is larger than the water gained in the cathode in Eq. 6, no

Table I. Geometrical, physical, and operating parameters.

Quantity	Value
Gas channel depth/width and shoulder width	0.5/1.0 and 1.0 mm
Catalyst layer/GDL/BP thickness, $\delta_{CL}/\delta_{GDL}/\delta_{BP}$	0.01/0.2/2.0 mm
Porosity of GDLs/catalyst layers, $\varepsilon_{GDL}/\varepsilon_{CL}$	0.6/0.5
Volume fraction of ionomer in catalyst layers, ε_m	0.23
Activation energy for oxygen reduction reaction, E_a[14]	73269 J/mol
Thermal conductivity of catalyst layer/GDL/BP, $k_{CL}^{eff}/k_{GDL}^{eff}/k_{BP}$[8,13]	3.0/3.0/20.0 W/mK
Specific heat of catalyst layer/GDL/membrane/BP, $c_p^{CL}/c_p^{GDL}/c_p^{m}$[14]	709/709/500 J/kg K
Density of ice/dry membrane, ρ_{ice}/ρ_m[18]	917/1980 kg/m^3
O_2 diffusivity in cathode gas at standard condition, $D_{M,0}^{O_2}$[18]	3.24×10^{-5} m^2/s
Net water transport per proton, α	0.1
Transfer coefficient, α_c[18]	1.0
Exchange current density $\times$ reaction surface area, $a_0 i_0^{c}$[8,18]	10000.0 A/m^3
RH of the fuel cell at initial state	50%
EW[8,18]	1.1
Latent heat of ice fusion, h_{fusion}	3.34×10^5 J/kg

ice forms in the cathode. Here, a dimensionless parameter of $\beta_{1,c}$ can be defined as

$$\beta_{1,c} = \frac{\dfrac{IA_m}{F}\dfrac{\xi_c(\bar{C}^w_{c,out} - \bar{C}^w_{c,in})}{4C^{O_2}_{c,in}}}{(1+2\alpha)\dfrac{I}{2F}A_m} = \frac{\xi_c(\bar{C}^w_{c,out} - \bar{C}^w_{c,in})}{2(1+2\alpha)C^{O_2}_{c,in}} \quad [8]$$

$\beta_{1,c}$ represents the ratio of the water removal rate by the cathode stream to the one gained by the cathode catalyst layer. If $\beta_{1,c}$ is less than one, there is a water accumulation in either the solid or ionomer phase in the cathode. A similar definition can also be made in the anode. Note that $\beta_{1,c}$ may be a function of time during transients and at steady state $\beta_{1,c}$ must be equal to 1. Under cold start or low-humidity operations, water is totally taken away by the gas flow (assuming no liquid/solid water in the stream). Therefore, it is especially of interest to only consider the gas flow in the channel

$$\beta_{1,c,g} = \frac{\xi_c(RH_{c,out}C^{sat}_{out} - RH_{c,in}C^{sat}_{in})}{2(1+2\alpha)C^{O_2}_{c,in}} \quad [9]$$

It can be seen that $\beta_{1,c,g}$ reaches its maximum value at $RH_{c,out} = 1$. Note that the temperatures at outlet and inlet are usually different (e.g., see Ref. 19). Here we only consider the cases with the same temperature at the inlet and outlet. The saturated concentration, $C^{sat}(T)$, can be calculated through the six-degree polynomial function proposed by Rasmussen,[20] which is accurate (relative error <0.0007) from -50 to 50°C. Figure 2 shows the plot of maximum $\beta_{1,c,g}$ at different temperatures and pressures (related to $C^{O_2}_{c,in}$). In the subzero startup, the value of $\beta_{1,c,g}$ is mostly very small ($<2\%$). Here, for analysis purposes, we neglect the water taken away by the gas flow in the following discussion.

In the catalyst layer below the freezing temperature, water molecules exist in gas, solid, and ionomer phases. The ionomer, typically Nafion, can hold much water as indicated by Ref. 9, which demonstrated that the amount of water in the membrane can be hundreds of times more than that in the gaseous phase of channel streams. Therefore, we can neglect the small amount of water in the

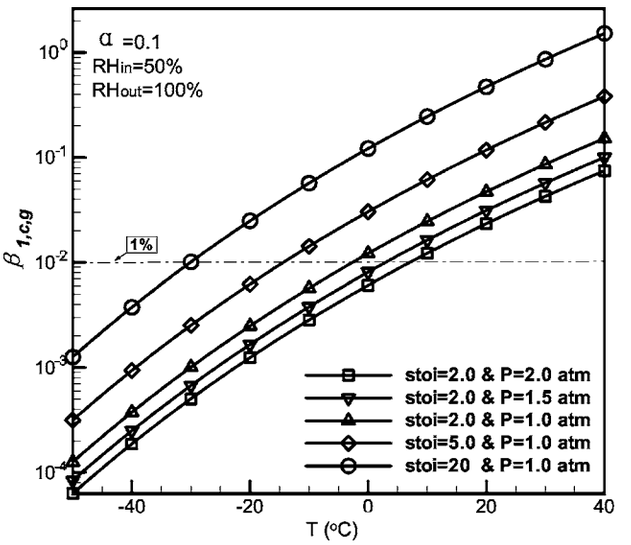

Figure 2. Functional dependence of $\beta_{1,c,g}$ on stoichiometric ratios and pressures.

gaseous phase in the catalyst layer. The cold start has two stages of operations before reaching the freezing point. One involves only membrane hydration in the catalyst layer; the other also includes the ice formation in the void space. The third stage starts when the fuel cell reaches 0°C, in which the residual ice in the catalyst layer melts. Assuming thermodynamic equilibrium between the gas and ionomer phases as well as between the ice and gas phases prevail due to the large phase interfacial area present within the porous catalyst layer, no solid water is produced at the first stage as the catalyst layer is partially hydrated, and the time constant, $\tau_{ice,1}$, for this stage can be calculated by

$$\int_0^{\tau_{ice,1}} S^w dt = \int_{\lambda_0}^{14} \varepsilon_m \frac{\rho_m}{EW} d\lambda \quad [10]$$

where ε_m is the volume fraction of the ionomer in the catalyst layer. Considering a constant S^w, $\tau_{ice,1}$ can be rewritten as

$$\tau_{ice,1} = \frac{\varepsilon_m \delta_{CL}\dfrac{\rho_m}{EW}(14-\lambda_0)}{(1+2\alpha)\dfrac{I}{2F}} = \frac{2F\rho_m\varepsilon_m\delta_{CL}(14-\lambda_0)}{EW(1+2\alpha)I} \quad [11]$$

Given the typical values of parameters for PEFCs, $\tau_{ice,1}$ is $\sim$10 s at 0.1 A/cm^2.

Assuming no liquid water at supercooled state forms, solid water is produced at $t > \tau_{ice,1}$ and the ice volume fraction in the void space, s_{ice}, can be expressed as

$$s_{ice}(t) = \frac{M^w}{\varepsilon_{CL}\rho_{ice}}\left(\int_{\tau_{ice,1}}^{t} S^w(t)dt - \int_{14}^{\lambda(t)} \varepsilon_m \frac{\rho_m}{EW} d\lambda\right) \quad [12]$$

For a constant S^w, neglecting the ionomer absorption in Eq. 12 (due to no liquid water present) yields

$$s_{ice}(t) = \frac{(1+2\alpha)M^w I}{2F\varepsilon_{CL}\rho_{ice}\delta_{CL}}(t-\tau_{ice,1}) = \frac{(t-\tau_{ice,1})}{\tau_{ice,2}} = \frac{t}{\tau_{ice,2}} - k_\tau$$
$$\tau_{ice,1} < t \le \tau_{ice,2} \quad [13]$$

where the time constant for the second stage, $\tau_{ice,2}$, and ratio of the two time constants, k_τ, are defined as

$$\tau_{\text{ice},2} = \frac{2F\varepsilon_{\text{CL}}\rho_{\text{ice}}\delta_{\text{CL}}}{(1+2\alpha)M^{\text{w}}I} \quad \text{and} \quad k_\tau = \frac{\tau_{\text{ice},1}}{\tau_{\text{ice},2}} = \frac{\rho_{\text{m}}\varepsilon_{\text{m}}(14-\lambda_0)M^{\text{w}}}{\rho_{\text{ice}}\varepsilon_{\text{CL}}\text{EW}} \tag{14}$$

k_τ is determined by the geometrical and material properties as well as initial membrane condition. Combining the two time constants yields

$$\tau_{s_{\text{ice}}} = \tau_{\text{ice},1} + \tau_{\text{ice},2} = \frac{2F\delta_{\text{CL}}}{(1+2\alpha)I}\left[\frac{\rho_{\text{m}}\varepsilon_{\text{m}}(14-\lambda_0)}{\text{EW}} + \frac{\varepsilon_{\text{CL}}\rho_{\text{ice}}}{M^{\text{w}}}\right] \tag{15}$$

This time constant $\tau_{s_{\text{ice}}}$ represents the time period for solid water to occupy the void space (i.e., $s_{\text{ice}} = 1$). Assuming the cell shuts down at $s_{\text{ice}} = 1$ (this might not hold true when tortuosity of the catalyst layer is sufficiently large; in that case, $\tau_{s_{\text{ice}}}$ can be defined as the time period for ice-volume fraction reaching the critical value), $\tau_{\text{T},1} > \tau_{s_{\text{ice}}}$ leads to failure of the startup due to the ice plug, while for $\tau_{\text{T},1} < \tau_{s_{\text{ice}}}$, the fuel cell is able to start up from a subzero environment. Therefore, one can further define a dimensionless parameter of β_2 as

$$\beta_2 = \frac{\tau_{\text{T},1}}{\tau_{s_{\text{ice}}}} \tag{16}$$

The PEFC is able to make a startup from subzero conditions upon $\beta_2 < 1$ and β_2 is independent of current densities. Once the cell temperature reaches 0°C, it starts decreasing due to fusion of the residual ice in the catalyst layer, and therefore there exists a maximum value of ice-volume fraction which can be calculated by

$$s_{\text{ice}}^{\max} = \frac{\tau_{\text{T},1}}{\tau_{\text{ice},2}} - k_\tau \tag{17}$$

To estimate the time constant of the ice fusion at 0°C, we can follow the approach of Eq. 3 and obtain $\tau_{\text{T},2}$ by solving

$$\int_{\tau_{\text{T},1}}^{\tau_{\text{T},1}+\tau_{\text{T},2}} I(E_{\text{o}}' - Vcell)dt = \rho_{\text{ice}}h_{\text{fusion}}\delta_{\text{CL}}\varepsilon_{\text{CL}}s_{\text{ice}}^{\max} = \rho_{\text{ice}}h_{\text{fusion}}\delta_{\text{CL}}\varepsilon_{\text{CL}}\left(\frac{\tau_{\text{T},1}}{\tau_{\text{ice},2}} - k_\tau\right) \tag{18}$$

Here E_{o}' is defined for the condition with liquid water at 0°C as product [approximately can use the (EMF) value of HHV for E_{o}']. Given the typical values of the parameters for PEFCs, $s_{\text{ice}}^{\max} = 1$ yields $\tau_{T,2} \sim 2.0$ s at 0.1 A/cm^2, which is fairly fast. We can then obtain s_{ice} through the following equation

$$s_{\text{ice}} = s_{\text{ice}}^{\max} - \frac{\int_{\tau_{\text{T},1}}^{t} I(E_{\text{o}}' - Vcell)dt}{\rho_{\text{ice}}h_{\text{fusion}}\delta_{\text{CL}}\varepsilon_{\text{CL}}} \quad \tau_{\text{T},1} < t \le \tau_{\text{T},1} + \tau_{\text{T},2} \tag{19}$$

Considering a constant rate of heat generation, we can simplify the expression as

$$s_{\text{ice}} = s_{\text{ice}}^{\max}\frac{\tau_{\text{T},2} + \tau_{\text{T},1} - t}{\tau_{\text{T},2}} = \left(\frac{\tau_{\text{T},1}}{\tau_{\text{ice},2}} - k_\tau\right)\frac{\tau_{\text{T},2} + \tau_{\text{T},1} - t}{\tau_{\text{T},2}} \quad \tau_{\text{T},1} < t \le \tau_{\text{T},1} + \tau_{\text{T},2} \tag{20}$$

Of course

$$s_{\text{ice}} = 0 \quad t > \tau_{\text{T},1} + \tau_{\text{T},2} \tag{21}$$

In addition, there coexist solid and liquid waters during $\tau_{\text{T},1} < t \le \tau_{\text{T},1} + \tau_{\text{T},2}$. At $t > \tau_{\text{T},1} + \tau_{\text{T},2}$, there is purely liquid water in the catalyst layer which may be able to transport to the GDL due to capillary action. Discussions of liquid-water transport are beyond the scope of this paper.

Analysis of cell voltage loss.— The solid water may cover the catalyst particles, therefore reducing the electrochemical active surface. The electrochemical kinetics is generally described by the Butler–Volmer equation

$$j_{\text{c}} = ai_{\text{o,T}}^{\text{c}}\left[\exp\left(\frac{\alpha_{\text{a}}}{RT}F\eta\right) - \exp\left(-\frac{\alpha_{\text{c}}}{RT}F\eta\right)\right] \tag{22}$$

where $i_{\text{o,T}}^{\text{c}}$ is the exchange current density, determined by the catalyst electrochemical kinetics, and a is the surface-to-volume ratio, describing the roughness of the porous electrodes. We follow the approach of the liquid-water impact on reaction surface and use the following empirical formula to account for the ice effect

$$a = (1 - s_{\text{ice}})^{\tau_{\text{a}}}a_0 \tag{23}$$

The coefficient, τ_a, is determined by the morphology of the solid water formed in the catalyst layer.

In PEFCs, the sluggish kinetics of oxygen reduction reaction (ORR) results in a high cathode overpotential. Thus, the Butler–Volmer equation can be well approximated by Tafel kinetics, i.e.

$$j_{\text{c}} = -ai_{\text{o,T}}^{\text{c}}\frac{C^{\text{O}_2}}{C^{\text{O}_2,\text{ref}}}\exp\left(-\frac{\alpha_{\text{c}}F}{\text{RT}}\eta\right) \tag{24}$$

where the surface overpotential is defined as

$$\eta = \Phi_{\text{s}} - \Phi_{\text{e}} - U_{\text{o}} \tag{25}$$

where Φ_{s} and Φ_{e} are electronic and electrolyte phase potentials, respectively, and the equilibrium potential, U_{o}, is a function of temperature

$$U_{\text{o}} = 1.23 - 0.9 \times 10^{-3}(T - 298) \tag{26}$$

In addition, temperature affects the ORR reaction rate and the exchange current density, $i_{\text{o,T}}^{\text{c}}$, which can be expressed in Arrhenius form as follows

$$i_{\text{o,T}}^{\text{c}} = i_{\text{o}}^{\text{c}}\exp\left[-\frac{E_{\text{a}}}{R}\left(\frac{1}{\text{T}} - \frac{1}{353.15}\right)\right] \tag{27}$$

where E_{a} denotes the activation energy for ORR at the Pt/Nafion electrode as provided by Parthasarathy et al.[21]

In transients, the output current density consists of the faradaic current of electrochemical reactions and the one from the double-layer charging or discharging

$$I = -j_{\text{c}}\delta_{\text{cl}} + I_{\text{db}} \tag{28}$$

The double layer occurs in a thin layer (of the order of nanometers) adjacent to the reaction interface and acts as a capacitor during the transience. Similar to porous electrodes of batteries, the double layer in the catalyst layer of a PEFC can be regarded as being in parallel to a charge-transfer-reaction resistor. The time constant of the double-layer charging/discharging was less than 1 ms.[9] The contribution from the double-layer charging/discharging can be estimated through the following equation

$$I_{\text{db}} \sim aC_{\text{db}}\frac{\Delta V_{\text{cell}}}{\Delta t}\delta_{\text{CL}} \tag{29}$$

Typically, the capacity C_{db} is around 20 μF/cm^2 and specific area, a, is about 10^3/cm, and ΔV_{cell} of $\sim$0.5 V and Δt of $\sim$100 s lead to I_{db} of $\sim$0.01 A/cm^2. The effect of double layer is small, $\sim$10% of typical operating current during cold start. For analysis purpose, we ignore the double-layer effect in this paper.

The solid water also hampers the transport of oxygen to reaction sites. The oxygen equation in one dimension can be expressed as

$$\frac{\partial\varepsilon C^{\text{O}_2}}{\partial t} + \frac{\partial u C^{\text{O}_2}}{\partial x} = \frac{\partial}{\partial x}\left[D^{\text{O}_2,\text{eff}}\frac{\partial C^{\text{O}_2}}{\partial x}\right] + S^{\text{O}_2} \tag{30}$$

Two types of diffusive transport are considered here. One is the molecular (or Fickian) diffusion, which takes place when the mean free length of molecules is relatively large compared with the pore

size. Under this circumstance, the molecules collide with each other during their passage through the pores, and hence the molecules move dependently of each other. In GDLs, molecular diffusion occurs and the coefficient is a function of temperature and pressure as described by

$$D_{\mathrm{M}}^{\mathrm{O}_2} = D_{\mathrm{M},0}^{\mathrm{O}_2}\left(\frac{T}{353}\right)^{3/2}\left(\frac{1}{P}\right) \quad [31]$$

The other is the Knudsen diffusion, which occurs in situations in which gas molecules collide more frequently with pore walls than with other gas molecules. This type of diffusion is encountered when the mean free path of gas molecules is of the order of the pore characteristic length scale. In the catalyst layer, the mean radius of the micropores[22] and the mean free path of the oxygen molecule ($\lambda_{\mathrm{molecule}} = 8\mathrm{RT}/\sqrt{2}\pi D^2 NaP$) are both ca 0.1 μm; therefore the Knudsen diffusion is an important mechanism of oxygen transport in the catalyst layer. The Knudsen diffusion coefficient in a long straight pore can be calculated through the kinetic theory of gases

$$D_{\mathrm{K}}^{\mathrm{O}_2} = \frac{2r_{\mathrm{pore}}}{3}\sqrt{\frac{8\mathrm{RT}}{\pi M^{\mathrm{O}_2}}} \quad [32]$$

The value of $D_{\mathrm{K}}^{\mathrm{O}_2}$ is around 2.64×10^{-5} m^2/s at $r_{\mathrm{pore}} = 0.1$ μm. Note that this value is comparable to the molecular one. To combine the two mechanisms, the harmonic mean is taken to calculate the average diffusivity. In addition, as the ice-volume fraction increases, the Knudsen diffusion becomes the dominant mechanism due to the decreasing pore radius. For analysis proposes, we denote the average diffusion coefficient in the catalyst layer as $D_{\mathrm{K}}^{\mathrm{O}_2}$ to distinguish from the one in GDLs where the molecular diffusion dominates. To account for the porosity and tortuosity factor, τ, of a porous media, the effective gas diffusion coefficient is given by

$$D^{\mathrm{O}_2,\mathrm{eff}} = \frac{\varepsilon}{\tau}D^{\mathrm{O}_2} = \varepsilon^{\tau_{\mathrm{d},0}}D^{\mathrm{O}_2} \quad [33]$$

where the Bruggeman factor, $\tau_{\mathrm{d},0}$, is constant, indicative of tortuosity of a porous medium. Note that the last term in Eq. 33 is also referred to as Bruggeman relation. In most of the previous work, the Bruggeman factor, $\tau_{\mathrm{d},0}$, is set to be a constant of 1.5. Wang et al.[23] indicated that the values of this factor for carbon paper and carbon cloth are different due to the difference in their pore structure.

In the presence of ice, the solid water attaches on the surface of the wall, narrowing the pore as well as changing the morphology of the solid matrix. To account for the effect of ice on diffusion, we follow the modeling approach in liquid-water transport and modify the coefficient as

$$D^{\mathrm{O}_2,\mathrm{eff}} = [\varepsilon(1 - s_{\mathrm{ice}})]^{\tau_{\mathrm{d}}}D^{\mathrm{O}_2} \quad [34]$$

Note that tortuosity factor, τ_{d}, also accounts for the effect of pore-size change on the Knudsen diffusion (see Eq. 32) and may be a function of the ice volume depending on morphology of the ice crystals.

Given no ice formation in the GDL, the time constant of the oxygen diffusion across the GDL can be estimated as

$$\tau_{\mathrm{diff}} = \frac{\delta_{\mathrm{GDL}}^2}{D_{\mathrm{GDL}}^{\mathrm{O}_2,\mathrm{eff}}} \quad [35]$$

The value of τ_{diff} is ~0.001 s for typical GDLs, which is fairly short. Therefore, the transient term of Eq. 30 can be neglected for oxygen transport in GDLs. In addition, ignoring the convection term in GDLs, the maximum drop of oxygen concentration across the GDL can be estimated by only considering the diffusive transport

$$\Delta C_{\mathrm{cGDL}}^{\mathrm{O}_2} = C_{\mathrm{cGDL}}^{\mathrm{O}_2} - C_{\mathrm{cCL}}^{\mathrm{O}_2} = \frac{I}{4F}\frac{\delta_{\mathrm{GDL}}}{D_{\mathrm{M}}^{\mathrm{O}_2,\mathrm{eff}}\varepsilon_{\mathrm{GDL}}^{\tau_{\mathrm{d},0}}} \quad [36]$$

At the current density of 0.1 A/cm^2 during cold start, $\Delta C_{\mathrm{GDL}}^{\mathrm{O}_2} < 0.1$ mol/m^3.

In the catalyst layer, assuming diffusion is the dominant transport mechanism and reaction rate is uniform, the oxygen profile can be obtained as

$$C^{\mathrm{O}_2} = C_{\mathrm{cCL}}^{\mathrm{O}_2} - \frac{I}{8F}\frac{\delta_{\mathrm{CL}}^2 - (x - x_{\mathrm{cCL}} + \delta_{\mathrm{CL}})^2}{\delta_{\mathrm{CL}}D_{\mathrm{K}}^{\mathrm{O}_2}[\varepsilon_{\mathrm{CL}}(1 - s_{\mathrm{ice}})]^{\tau_{\mathrm{d}}}} = C_{\mathrm{cCL}}^{\mathrm{O}_2}\left[1 - Da\frac{1 - \left(\frac{x - x_{\mathrm{cCL}}}{\delta_{\mathrm{CL}}} + 1\right)^2}{\varepsilon_{\mathrm{CL}}^{\tau_{\mathrm{d}} - \tau_{\mathrm{d},0}}[(1 - s_{\mathrm{ice}})]^{\tau_{\mathrm{d}}}}\right] \quad [37]$$

where the dimensionless parameter, *Da*, is called the Damköhler number defined as

$$Da = \frac{I}{8F}\frac{\delta_{\mathrm{CL}}}{C_{\mathrm{cCL}}^{\mathrm{O}_2}D_{\mathrm{K}}^{\mathrm{O}_2}\varepsilon^{\tau_{\mathrm{d},0}}} = \frac{\text{Reaction rate}}{\text{Mass-transport rate}} \quad [38]$$

Current density of 0.1 A/cm^2, P of 1.0 atm, and T of −30°C yield $Da \sim 1.3 \times 10^{-4}$. Note that several key parameters, such as operating pressure, stoichiometric ratio, current density, and catalyst layer thickness, are lumped in *Da*. It is of interest to evaluate the oxygen concentration drop across the catalyst layer

$$\Delta C_{\mathrm{cGDL}}^{\mathrm{O}_2} = C_{\mathrm{cCL}}^{\mathrm{O}_2} - C_{\mathrm{cMEM}}^{\mathrm{O}_2} = Da\frac{C_{\mathrm{cCL}}^{\mathrm{O}_2}}{\varepsilon_{\mathrm{CL}}^{\tau_{\mathrm{d}} - \tau_{\mathrm{d},0}}(1 - s_{\mathrm{ice}})^{\tau_{\mathrm{d}}}} \quad [39]$$

which is small (<0.5 mol/m^3) at 0.1 A/cm^2, $\tau_{\mathrm{d},0} = \tau_{\mathrm{d}} = 1.5$, and $s_{\mathrm{ice}} < 0.98$. Therefore, the solution of Eq. 37 is valid at s_{ice} up to 98%. When s_{ice} reaches a level that causes serious starvation (therefore j_{c} is no longer uniform and the transient term cannot be neglected), the solution, Eq. 37, can be invalid. In that case, the oxygen profile can be obtained by coupling Eq. 24 and 30.

Substituting Eq. 37 into Eq. 24 yields

$$\eta(s_{\mathrm{ice}},x) = -\frac{\mathrm{RT}}{\alpha_{\mathrm{c}}F}\ln\left\{\frac{IC_{\mathrm{O}_2,\mathrm{ref}}}{a_0 i_{0,\mathrm{c}}^{\mathrm{ref}}\delta_{\mathrm{CL}}C_{\mathrm{cCL}}^{\mathrm{O}_2}}\left[(1 - s_{\mathrm{ice}})^{\tau_{\mathrm{a}}}\left(1 - Da\frac{1 - \left(\frac{x - x_{\mathrm{cCL}}}{\delta_{\mathrm{CL}}} + 1\right)^2}{\varepsilon_{\mathrm{CL}}^{\tau_{\mathrm{d}} - \tau_{\mathrm{d},0}}(1 - s_{\mathrm{ice}})^{\tau_{\mathrm{d}}}}\right)\right]^{-1}\right\} \quad [40]$$

Therefore, a dimensionless function can be defined as

$$\Pi(s_{\mathrm{ice}},x) = \ln\left[(1 - s_{\mathrm{ice}})^{\tau_{\mathrm{a}}}\left(1 - Da\frac{1 - \left(\frac{x - x_{\mathrm{cCL}}}{\delta_{\mathrm{CL}}} + 1\right)^2}{\varepsilon_{\mathrm{CL}}^{\tau_{\mathrm{d}} - \tau_{\mathrm{d},0}}(1 - s_{\mathrm{ice}})^{\tau_{\mathrm{d}}}}\right)\right] \quad [41]$$

It can be seen that impacts of the solid water are solely contained in the function Π. The function Π consists of two parts: one is from the reduction of electrochemical active surface due to solid water coverage, and the other is oxygen starvation. Then Eq. 40 can be written as

$$\eta(s_{\mathrm{ice}},x) = -\frac{\mathrm{RT}}{\alpha_{\mathrm{c}}F}\ln\left[\frac{IC^{\mathrm{O}_2,\mathrm{ref}}}{a_0 i_{0,\mathrm{c}}^{\mathrm{ref}}\delta_{\mathrm{CL}}C_{\mathrm{cCL}}^{\mathrm{O}_2}}\right] + \frac{\mathrm{RT}}{\alpha_{\mathrm{c}}F}\Pi(s_{\mathrm{ice}},x) = \eta_{\mathrm{c,o}} + \Delta\eta_{\mathrm{c}} \quad [42]$$

where

$$\eta_{\mathrm{c,o}} = -\frac{\mathrm{RT}}{\alpha_{\mathrm{c}}F}\ln\left[\frac{IC^{\mathrm{O}_2,\mathrm{ref}}}{a_0 i_{0,\mathrm{c}}^{\mathrm{ref}}\delta_{\mathrm{CL}}C_{\mathrm{cCL}}^{\mathrm{O}_2}}\right] \quad \text{and} \quad \Delta\eta_{\mathrm{c}} = \frac{\mathrm{RT}}{\alpha_{\mathrm{c}}F}\Pi(s_{\mathrm{ice}},x) \quad [43]$$

$\eta_{\mathrm{c,o}}$ denotes the overpotential at the interface between the cathode catalyst layer and GDL when no ice is present. The overpotential change due to ice presence can be further expressed as

$$\Delta\eta_{\mathrm{c}}(s_{\mathrm{ice}},x) = \Delta\eta_{\mathrm{c},1} + \Delta\eta_{\mathrm{c},2} \quad [44]$$

where

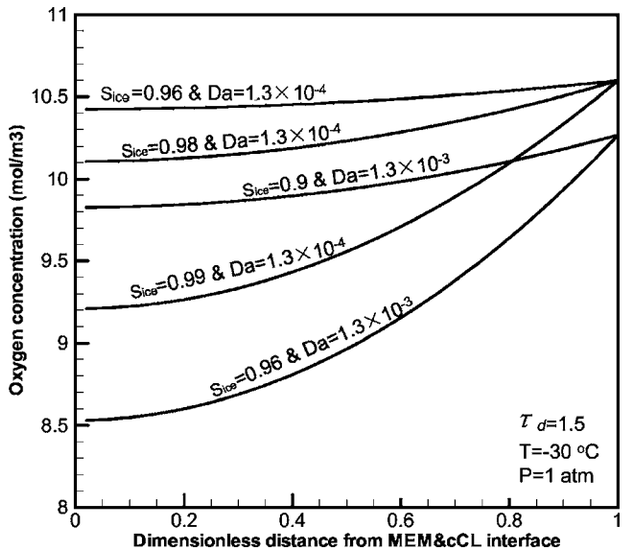

Figure 3. Oxygen profiles in the cathode catalyst layer at different ice-volume fractions and *Da*'s.

$$\Delta\eta_{c,1} = \tau_a \frac{RT}{\alpha_c F} \ln(1 - s_{ice})$$

$$\Delta\eta_{c,2} = \frac{RT}{\alpha_c F} \ln\left[1 - Da \frac{1 - \left(\frac{x - x_{cCL}}{\delta_{CL}} + 1\right)^2}{\varepsilon_{CL}^{\tau_d - \tau_{d,0}}(1 - s_{ice})^{\tau_d}}\right] \quad [45]$$

$\Delta\eta_{c,1}$ and $\Delta\eta_{c,2}$ represent the voltage losses due to the reactive surface reduction and oxygen starvation, respectively. Therefore, a dimensionless parameter β_3 can be defined as the ratio of these two

$$\beta_3 = \frac{\Delta\eta_{c,1}}{\Delta\eta_{c,2}} \quad [46]$$

In addition, we can evaluate the voltage loss due to oxygen starvation by considering the location at the interface between the membrane and catalyst layer

$$\Delta\eta_{c,2}(s_{ice}, x_{cCL} - \delta_{CL}) = \frac{RT}{\alpha_c F} \ln\left(1 - \frac{Da}{\varepsilon_{CL}^{\tau_d - \tau_{d,0}}(1 - s_{ice})^{\tau_d}}\right) \quad [47]$$

Another important factor is the sensitivities of $\Delta\eta_{c,1}$ and $\Delta\eta_{c,2}$ to s_{ice}, defined as

$$k_{\eta_{c,1}} = \left|\frac{\partial\Delta\eta_{c,1}}{\partial s_{ice}}\right| \quad \text{and} \quad k_{\eta_{c,2}} = \left|\frac{\partial\Delta\eta_{c,2}}{\partial s_{ice}}\right| \quad [48]$$

Once the cathode overpotential is calculated, the cell voltage can be obtained through

$$V_{cell} = U_o + \eta_c - \eta_a - R_\Omega I \quad [49]$$

Assuming no ice in the anode during cold start, η_a can be neglected at low current density. The last term on the right side represents voltage loss due to ohmic resistance. It consists of the ionic resistances in the membrane and catalyst layers and electronic one, as well as contact resistance. R_Ω can be calculated through

$$R_\Omega = \frac{\delta_m}{\kappa_m} + \frac{\delta_{aCL}}{2\kappa_{aCL}\varepsilon_m^{\tau_k}} + \frac{\delta_{cCL}}{2\kappa_{cCL}\varepsilon_m^{\tau_k}} + R_{e-} + R_{contact} \quad [50]$$

Usually, R_{e-} is small and negligible.

Results and Discussion

Figure 3 shows the oxygen profiles in the catalyst layer at different levels of the ice-volume fraction with a constant value of tortuosity ($\tau_{d,0} = \tau_d = 1.5$) in the catalyst layer. The oxygen concentration undergoes a fairly small decrease (<0.5 mol/m^3 or $<5\%$) in the catalyst layer for the ice-volume fraction up to 98% for *Da* = 1.3×10^{-4} at 0.1 A/cm^2. When the ice fraction reaches 99%, the oxygen concentration inside the catalyst layer starts to decrease by a considerable value (~ 1 mol/m^3). As to *Da* = 1.3×10^{-3} (e.g., *I* = 1.0 A/cm^2), the drop is small at the ice-volume fraction up to 90%. In addition, the oxygen-concentration value at the interface between the catalyst layer and GDL is smaller at the larger *Da* due to a higher current density considered for *Da* = 1.3×10^{-3}. The magnitude of the concentration drop within the GDL can be estimated through Eq. 36.

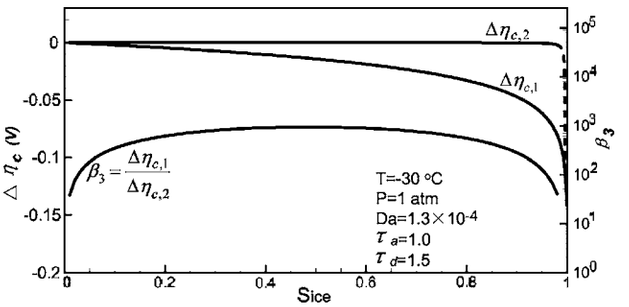

Figure 4. Profiles of $\Delta\eta_{c,1}$, $\Delta\eta_{c,2}$ (at the interface between the membrane and cathode catalyst layer) and their ratio, β_3, at -30°C, $\tau_a = 1$ and $\tau_d = 1.5$.

Figure 4 presents the profiles of $\Delta\eta_{c,1}$ and $\Delta\eta_{c,2}$ as well as their ratio β_3 at -30°C. The magnitude of $\Delta\eta_{c,1}$ increases steadily with ice-volume fraction, while that of $\Delta\eta_{c,2}$ is fairly small except near $s_{ice} = 1$. $\Delta\eta_{c,1}$ is several orders of magnitude larger than $\Delta\eta_{c,2}$ in a large range of the ice-volume fraction. At very high ice fraction ($>95\%$), $\Delta\eta_{c,2}$ starts to increase dramatically. In addition, the trend of the parameter, β_3, shows an increase at first to about thousands, followed by a decrease at the very end. Reduction in the reactive surface due to ice coverage is a major mechanism leading to the voltage loss during cold start.

Note that the above conclusions are based on a constant tortuosity factor, $\tau_d = 1.5$. Figure 5 shows the $\Delta\eta_{c,2}$ profiles at different tortuosities and *Da*s. The value of *Da* has a small effect on the curve of $\Delta\eta_{c,2}$ and it only slightly moves the starting point of oxygen starvation ahead, while the tortuosity of the catalyst layer has great impact on the voltage loss. Under the tortuosity of 4.0, $\Delta\eta_{c,2}$ starts to dramatically increase its magnitude around $s_{ice} = 0.8$.

Figure 6 displays the profiles of sensitivities of $\Delta\eta_{c,1}$ and $\Delta\eta_{c,2}$, i.e., $k_{\eta_{c,1}}$ and $k_{\eta_{c,2}}$, at different τ_d and τ_a. Here, we assume τ_d and τ_a are independent of s_{ice}. It can be seen that both values increase dramatically as s_{ice} approaches unity, and $k_{\eta_{c,2}}$ is much smaller than $k_{\eta_{c,1}}$ in most of the region except s_{ice} close to 1. In addition, $k_{\eta_{c,1}}$ is

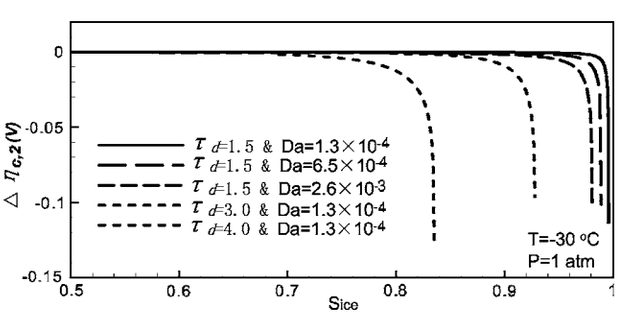

Figure 5. Profiles of $\Delta\eta_{c,2}$, at the interface between the membrane and cathode catalyst layer for different τ_d and *Da*'s.

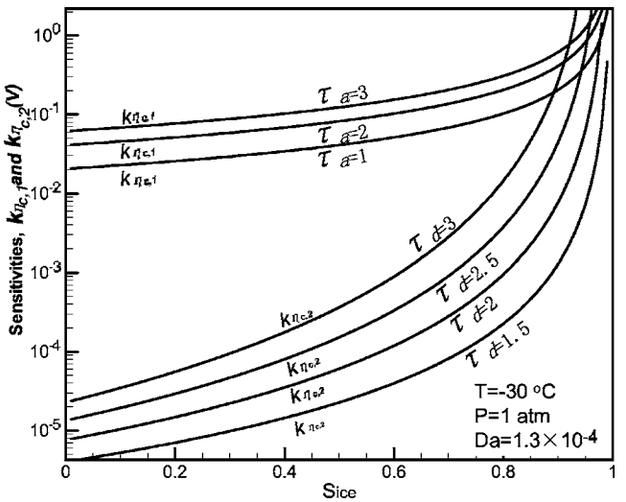

Figure 6. Profiles of sensitivities, $\Delta\eta_{c,1}$ and $\Delta\eta_{c,2}$ at different τ_d and τ_a.

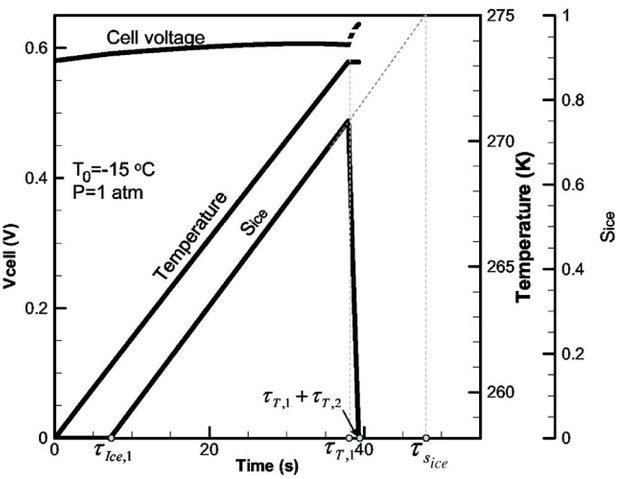

Figure 8. Evolution of temperature, ice-volume fraction, and cell voltage during cold start from −15°C.

linear with τ_a, as shown in Eq. 45 and 48, while τ_d is nonlinear with $k_{\eta_{c,2}}$ and has a profound impact on the value of the latter.

Figure 7 shows the evolution of temperature, ice-volume fraction, and cell voltage during cold start from −30°C with the time constants indicated in the plot. In this case, $\beta_2 = \frac{\tau_{T,1}}{\tau_{S_{ice}}} > 1$ and the ice-volume fraction reaches unity before the cell temperature increases to 0°C, therefore the startup fails. Due to a constant current density of 0.1 A/cm^2 considered, the ice-volume fraction increases almost linearly after the operation is beyond the time constant of membrane hydration, $\tau_{ice,1}$. The cell temperature also displays a nearly linear increase with time. As to the cell voltage, it first increases due to increasing temperature, which benefits the reaction kinetics and transport mechanisms. As the ice-volume fraction further increases, the cell-voltage change is then dominated by the reduction of electrochemical active surface and oxygen starvation, leading to a fast drop in cell voltage.

Figure 8 shows the startup of the fuel cell from −15°C. In this case, $\beta_2 < 1$, therefore the cell temperature increases to 0°C before the ice-volume fraction reaches unity. The temperature stays constant at 0°C for a short while due to fusion of the residual ice. Simultaneously, the ice-volume fraction decreases with time, resulting in the voltage increases. However, this model does not account for liquid-water effect, which may have a profound effect on catalyst-layer performance; therefore the slight increase in cell voltage during the fusion process is drawn by a dashed line. The fuel cell used in Ref. 2 needs external heating sources in order to make a startup below −5°C. From the previous analysis and Fig. 7 and 8, it can be seen that β_2 is the key parameter that determines if fuel cells are able to start successfully. The fuel cell in Ref. 2 has a deeper gas channel (1 mm), which may lead to a larger value of the effective length of bipolar plates δ_{BP} and hence $\tau_{T,1}$ (see Eq. 4).

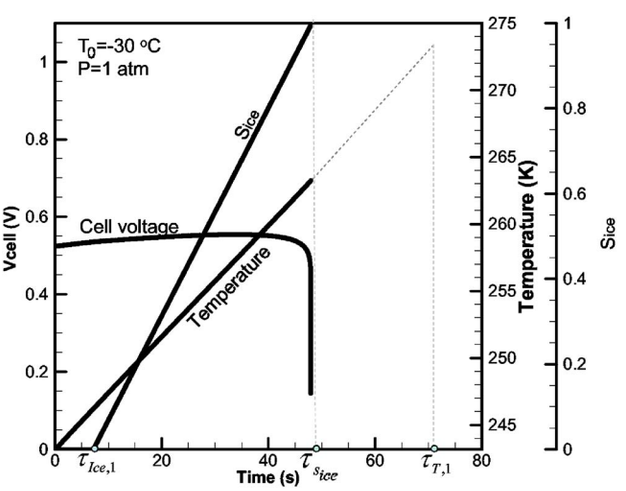

Figure 7. Evolution of temperature, ice-volume fraction, and cell voltage during cold start from −30°C.

Conclusion

This paper investigated the electrochemical and transport phenomena in the cathode catalyst layer of fuel cells during startup from subzero environments. We found that the spatial variation of temperature in a fuel cell is small and negligible under low current densities during cold start, and thereby a lumped parameter thermal model was developed for PEFCs. In addition, one-dimensional analysis indicated that the concentration drop of oxygen within the catalyst layer is fairly small when the ice-volume fraction and tortuosity of the catalyst layer are at moderate levels. A high value of tortuosity has a profound impact on reactant starvation in the catalyst layer during cold-start. In addition, we defined a number of key parameters that govern the cold-start operations and investigated their impacts on cell performance. These parameters are extremely important for cell designs and controls for PEFC cold start. Finally, we found that reduction in the electrochemical active surface of the catalyst may be a major mechanism leading to the cell voltage loss during cold start.

Acknowledgments

Partial support of this work by the UC Irvine Academic Senate Council on Research, Computing and Library Resources (CORCLR) is gratefully acknowledged.

The University of California, Irvine assisted in meeting the publication costs of this article.

List of Symbols

A_m	electrode area, m^2
a	water activity; effective catalyst area per unit volume, m^2/m^3
a_o	catalyst surface area per unit volume, m^2/m^3
BP	bipolar plate
C	capacitance of double layer, mF/cm^2; molar concentration of species k, mol/m^3
C_p	specific heat, J/kg K

D	species diffusivity, m^2/s; diameter of molecule, m
EW	equivalent weight of dry membrane, kg/mol
F	Faraday's constant, 96,487 C/equivalent
I	current density, A/cm^2
i	superficial current density, A/cm^2
j	transfer current density, A/cm^3
k	thermal conductivity, W/m K; sensitivity of overpotential, V
K	Knudsen diffusion
M	molecular weight, kg/mol; molecular diffusion
Na	Avogadro's number
n	the direction normal to the surface
n_d	electro-osmotic coefficient, H_2O/H^+
P	pressure, Pa
$\dot{Q}$	rate of heat transfer
r	radius, m
R	universal gas constant, 8.134 J/mol K; ohmic resistance, $m\Omega\ cm^2$
RH	relative humidity
S	source term
s_{ice}	ice volume fraction
$d\vec{s}$	differential element of surface area
t	time, s
T	temperature, K
U_o	equilibrium potential, V
$\vec{\mathbf{u}}$	velocity vector, m/s
V	volume, m^3

Greek

α	transfer coefficient; net water flux per proton flux
β	dimensionless parameter
ρ	density, kg/m^3
ϕ	phase potential, V
κ	proton conductivity, S/m
ξ	stoichiometric flow ratio
λ	membrane water content
ε	porosity
η	surface overpotential, V
τ	tortuosity; time constant, s
δ	thickness, m

Superscripts and subscripts

c	cathode
CL	catalyst layer
d	diffusion
db	double layer
e	electrolyte
eff	effective value
g	gas phase
GDL	gas diffusion layer
m	membrane phase
o	reference value; initial value
ref	reference value
s	solid
sat	saturate value
sg	phase change between ice and water vapor
w	water

References

1. C. Y. Wang, *Chem. Rev. (Washington, D.C.)*, **104**, 4727 (2004).
2. Y. Hishinuma, T. Chikahisa, F. Kagami, and T. Ogawa, *JSME Int. J., Ser. B*, **47**, 235 (2004).
3. R. C. McDonald, C. K. Mittelsteadt, and E. L. Thompson, *Fuel Cells*, **4**, 208 (2004).
4. E. Cho, J. J. Ko, H. Y. Ha, S. A. Hong, K. Y. Lee, T. W. Lim, and I. H. Oh, *J. Electrochem. Soc.*, **151**, A661 (2004).
5. M. Oszcipok, D. Riemann, U. Kronenwett, M. Kreideweis, and M. Zedda, *J. Power Sources*, **145**, 407 (2005).
6. Q. Yana, H. Toghianib, Y.-W. Leea, K. Liangb and H. Causey, *J. Power Sources*, **160**, 1242 (2006).
7. S. He and M. M. Mench, *J. Electrochem. Soc.*, **153**, A1724 (2006).
8. L. Mao and C. Y. Wang, *J. Electrochem. Soc.*, **154**, B341 (2007).
9. Y. Wang and C. Y. Wang, *Electrochim. Acta*, **50**, 1307 (2005).
10. Y. Wang and C. Y. Wang, *Electrochim. Acta*, **51**, 3924 (2006).
11. M. Saito, K. Hayamizu, and T. Okada, *J. Phys. Chem. B*, **109**, 3112 (2005).
12. M. Cappadonia, J. W. Erning, S. M. S. Niaki, and U. Stimming, *Solid State Ionics*, **77**, 65 (1995).
13. Y. Wang and C. Y. Wang, *J. Electrochem. Soc.*, **153**, A1193 (2006).
14. Y. Wang and C. Y. Wang, *J. Electrochem. Soc.*, **154**, B636 (2007).
15. J. Larminie and A. Dicks, *Fuel Cell Systems Explained*, 2nd ed., John Wiley & Sons, New York (2003).
16. Y. Wang and C. Y. Wang, *J. Electrochem. Soc.*, **152**, A445 (2005).
17. J. S. Yi and T. V. Nguyen, *J. Electrochem. Soc.*, **146**, 38 (1999).
18. Y. Wang and C. Y. Wang, *J. Power Sources*, **147**, 148 (2005).
19. Y. Wang and C. Y. Wang, *J. Power Sources*, **153**, 130 (2006).
20. L. A. Rasmussen, *J. Appl. Meteorol.*, **17**, 1564 (1978).
21. A. Parthasarathy, S. Srinivasan, and A. J. Appleby, *J. Electrochem. Soc.*, **139**, 2530 (1992).
22. M. C. Tucker, M. Odgaard, P. B. Lund, S. Yde-Andersen, and J. O. Thomas, *J. Electrochem. Soc.*, **152**, A1844 (2005).
23. Y. Wang, C. Y. Wang, and K. S. Chen, *Electrochim. Acta*, **52**, 3965 (2007).